



Contents lists available at ScienceDirect

Spectrochimica Acta Part A: Molecular and Biomolecular Spectroscopy

journal homepage: www.elsevier.com/locate/saa

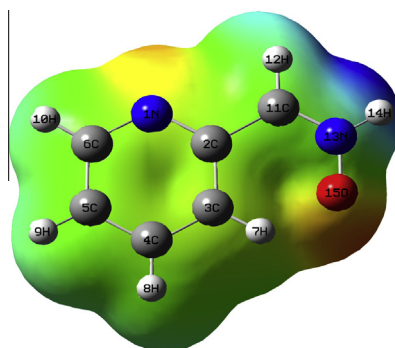
Vibrational frequency analysis, FT-IR, FT-Raman, ab initio, HF and DFT studies, NBO, HOMO–LUMO and electronic structure calculations on pycolinaldehyde oxime

A. Suvitha^{a,b,*}, S. Periandy^c, S. Boomadevi^d, M. Govindarajan^e^a Periyar Maniyammai University, Vallam, Thanjavur, India^b St. Francis College, Bangalore, India^c Department of Physics, Tagore Arts College, Puducherry, India^d Department of Physics, Periyar Maniyammai University, Vallam, Thanjavur, India^e Department of Physics, MGGA College, Mahe, Puducherry, India

HIGHLIGHTS

- Spectroscopic properties of pycolinaldehyde oxime were examined by FT-IR, FT-Raman and NMR techniques, HF and DFT methods.
- NLO and NBO analysis of the molecule were studied.
- NMR chemical shift of the molecule were studied.
- HOMO and LUMO energies, Molecular electrostatic potential distribution of the molecule were calculated.

GRAPHICAL ABSTRACT



ARTICLE INFO

Article history:

Received 31 May 2013

Received in revised form 7 July 2013

Accepted 21 July 2013

Available online 6 August 2013

Keywords:

HF

DFT

Pycolinaldehyde Oxime (PAO)

NBO analysis

HOMO

LUMO

ABSTRACT

In this work, the vibrational spectral analysis is carried out by using Raman and infrared spectroscopy in the range 100–4000 cm^{-1} and 50–4000 cm^{-1} , respectively, for pycolinaldehyde oxime (PAO) ($\text{C}_6\text{H}_6\text{N}_2\text{O}$) molecule. The vibrational frequencies have been calculated and scaled values are compared with experimental FT-IR and FT-Raman spectra. The structure optimizations and normal coordinate force field calculations are based on HF and B3LYP methods with 6-311++G(d,p) basis set. The results of the calculation shows excellent agreement between experimental and calculated frequencies in B3LYP/6-311++G(d,p) basis set. The optimized geometric parameters are compared with experimental values of PAO. The non linear optical properties, NBO analysis, thermodynamics properties and mulliken charges of the title molecule are also calculated and interpreted. A study on the electronic properties, such as HOMO and LUMO energies, are performed by time-dependent DFT (TD-DFT) approach. Besides, frontier molecular orbitals (FMO), molecular electrostatic potential (MEP) are performed. The effects due to the substitutions of $\text{CH}=\text{NOH}$ ring are investigated. The ^1H and ^{13}C nuclear magnetic resonance (NMR) chemical shifts of the molecule are calculated by the gauge independent atomic orbital (GIAO) method and compared with experimental results.

© 2013 Elsevier B.V. All rights reserved.

Introduction

Pyridine-2-carbaldehyde oxime has the general formula is $\text{C}_6\text{H}_6\text{N}_2\text{O}$. Usually it is a white to pale pink powder, belongs to a

* Corresponding author. Tel.: +91 9632814332.

E-mail address: suvidanam@gmail.com (A. Suvitha).

family of compounds called oximes (Fig. 1). Molecular weight of PAO is 122.125 (g/mol) with 1-H bond donor and 3-H bond acceptor. PAO is a frequently used ligand in synthesis of metal complexes [1–3]. Oxime pyridines are widely used in pharmacological and medical applications [4]. Pyridine compounds have been used as nonlinear materials and photo chemicals widely used as anticancer drugs, antihypertension, antifungal reagents, pesticides, herbicides, plant growth reagents, etc. [5]. PAO has an important role in reversing paralysis of the respiratory muscles but due to its poor blood-brain barrier penetration, it has little effect on centrally-mediated respiratory depression [6]. Many substituted pyridines are involved in bioactivities with applications in pharmaceutical drugs and agricultural products [7–9]. The picoline derivatives prepared from aminopyridine derivatives have been shown to have cholesterol lowering properties, anticancer and anti-inflammatory agents [7]. The ring nitrogen of most pyridines undergoes reactions such as protonation, alkylation and acylation [8]. The harmonic frequencies of pyridine derivatives are calculated by several authors [10–12].

To the best of our knowledge, neither quantum chemical calculations, nor the vibrational analysis study of Picolinaldehyde oxime (abbreviated as PAO) has been reported yet. This inadequacy observed in the literature encouraged us to make this theoretical and experimental vibration spectroscopic research based on the structure of molecule to give a correct assignment of the fundamental bands in experimental FT-IR and FT-Raman spectra were found the spectrum varies significantly, which indicated the changing of molecule structure. Therefore, a few modes with different system structure were set up for calculation. At present, there are many papers about theoretical research: studies of vibration assignment on substituted pyridine because of pharmaceutical application [13,14]. The understanding of their molecular properties as well as natures of reaction mechanism they undergo has got great importance. Hence, the investigation on the structures and the vibrations of pyridine and substituted pyridine are still being carried out, increasingly.

Experimental

The compound under investigation namely PAO is purchased from M/S Aldrich Chemicals, USA with spectroscopic grade and it is used as such without any further purification. The FT-IR spectrum of the compound has been recorded in Perkin-Elmer 180



Fig. 1. Sample picture of picolinaldehyde oxime.

Spectrometer between 4000 and 100 cm^{-1} . The spectral resolution is $\pm 2 \text{ cm}^{-1}$. The FT-Raman spectrum of the compound is also recorded in the same instrument with FRA 106 Raman module equipped with Nd: YAG laser source operating at 1.064 μm line widths with 200 mW powers. The spectra are recorded with scanning speed of 30 $\text{cm}^{-1} \text{ min}^{-1}$ of spectral width 2 cm^{-1} . The frequencies of all sharp bands are accurate to $\pm 1 \text{ cm}^{-1}$.

Chemical composition of molecule

PAO is synthesized by reacting picolinaldehyde (2-formyl pyridine) with hydroxylamine, giving pyridine-2-aldoxime [15]. From Fig. 2, the following mechanism may also be postulated: nucleophilic displacement of the chloro group yields the alkylhydroxylamine (I), subsequent protonation of the hydroxyl group of I to produce II, followed by the elimination, yields the aldimine (III), and the aldimine in the presence of excess hydroxylamine yields the product oxime (IV) [16].

Quantum chemical calculations

The entire quantum chemical calculations have been performed at HF and DFT (B3LYP) methods with 6-311++G(d,p) basis set using the Gaussian 03 program [17]. The optimized structural parameters have been evaluated for the calculations of vibrational frequencies by assuming C_s point group symmetry. At the optimized geometry for the title molecule no imaginary frequency modes were obtained, so there is a true minimum on the potential energy surface was found. As a result, the unscaled calculated frequencies, reduced masses, force constants, infrared intensities, and Raman activities are obtained. In order to fit the theoretical wave numbers to the experimental, the scaling factors have been introduced by using a least square optimization of the computed to the experimental data. Vibrational frequencies are scaled as 0.9067 for HF and the range of wavenumbers above 1700 cm^{-1} are scaled as 0.958 and below 1700 cm^{-1} scaled as 0.983 for B3LYP to account for systematic errors caused by basis set incompleteness, neglect of electron correlation and vibrational anharmonicity [18]. After scaled with the scaling factor, the deviation from the experiments is less than 10 cm^{-1} with a few exceptions. Gauss view Program has been considered to get visual animation and for the verification of the normal modes assignment [19,20]. The electronic absorption spectra for optimized molecule calculated with the time dependent DFT (TD-DFT) at B3LYP/6-311++G(d,p) and HF/6-311++G(d,p) level at in gas phase. Furthermore, in order to show nonlinear optic (NLO) activity of title molecule, the dipole moment, linear polarizability and first hyperpolarizability were obtained. Moreover, the changes in the thermodynamic functions

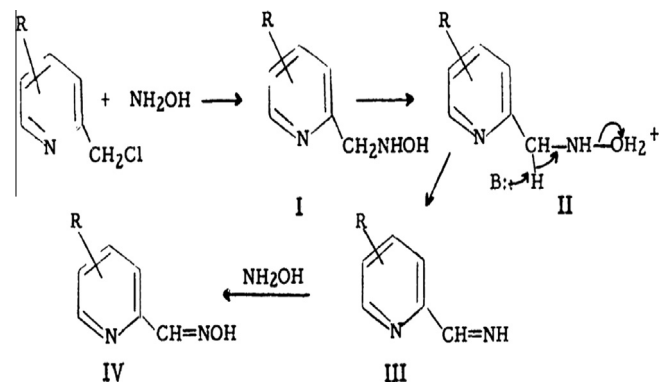


Fig. 2. Chemical composition of picolinaldehyde oxime.

(the heat capacity, entropy, and enthalpy) were investigated for the different temperatures from the vibrational frequency calculations of title molecule.

Results and discussion

Molecular geometry

The optimized geometry of PAO which performed by HF and B3LYP methods with atoms numbering are shown in Fig. 3. The optimized bond lengths, and bond angles of title compound which are calculated by using ab-initio HF and DFT(B3LYP) methods with 6-311++G(d,p) basis set are shown in Table S1. In this work, geometry optimization parameters for PAO have been employed without symmetry constrains. The carbon atoms are bonded to the hydrogen atoms with π and σ bond in pyridine and the substitution of an oxime for hydrogen reduces the electron density at the ring carbon atom. The ring carbon atoms in substituted pyridine exert a larger attraction on the valence electron cloud of the hydrogen atom resulting in an increase in the C–H force constant and a decrease in the corresponding bond length. The reverse holds well on substitution with electron donating groups.

From Table S1, the C–H bond lengths are shorter than experimental values (1.081 Å) for both B3LYP and HF methods. The actual change in the C–H bond length would be influenced by the combined effects of the inductive–mesmeric interaction and the electric dipole field of the polar substituent. C–C bond lengths are calculated by HF method are little shorter than DFT/B3LYP method compared with experimental value. Bond length of C2–C3 and C5–C6 for HF is 1.390 Å but for DFT 1.402 Å, which is closer to the experimental data (1.395 Å), where as the other C–C bonds are like C3–C4, and C4–C5 ~ 1.396 Å in DFT/B3LYP respectively. The average bond distances of C–C and C–H in the pyridine ring calculated by DFT method are 1.395 and 1.070 Å, respectively. The bond lengths of C–C bond are differing in value, which is due to the substitutions on the benzene ring in the place of hydrogen atom. The optimized N–H bond length are calculated 1.000 Å by B3LYP and 1.007 Å by HF with 6-311++G(d,p) method. By comparing those values with experimental value of 1.001 Å, it is observed that B3LYP estimate the N–H bond length better than HF, which underestimates this bond than experimental values. The optimized C–N bond length by two methods are 1.344 and 1.344 Å for B3LYP/6-311+G(d,p) and 1.331 and 1.313 Å for

HF/6-311+G(d,p) methods, respectively. The C–N bond lengths are shorter than experimental values (1.388 Å) and B3LYP values are closer than HF values. The ring appears little distorted and angles slightly out of perfect hexagonal structure. The asymmetry of the pyridine ring is also evident from the positive deviation of C4–C5–C6 and C2–C3–C4 angles which are calculated 119.4 Å (B3LYP) and the C3–C2–C11 angle found to be bigger than calculation (1.1 Å). Substitution with the oxime leads to some changes of the bond angles in the aromatic ring. The C–C–H angles are almost same with (120.4 Å) except C3–C4–H8 and C5–C4–H8 [21].

NLO activity

The second-order polarizability or first hyperpolarizability β , dipole moment μ and polarizability α is calculated using 6-311++G(d,p) basis set on the basis of the finite-field approach. The complete equations for calculating the magnitude of total dipole moment μ , the mean polarizability α_0 , the anisotropy of the polarizability $\Delta\alpha$ and the mean first polarizability β , using the x, y, z components from Gaussian 03 W output is as follows

$$\mu_{\text{tot}} = (\mu_x^2 + \mu_y^2 + \mu_z^2)^{\frac{1}{2}}$$

$$\alpha_{\text{tot}} = \frac{1}{3} (\alpha_{xx} + \alpha_{yy} + \alpha_{zz})$$

$$\Delta\alpha = \frac{1}{\sqrt{2}} \left[(\alpha_{xx} - \alpha_{yy})^2 + (\alpha_{yy} - \alpha_{zz})^2 + (\alpha_{zz} - \alpha_{xx})^2 + 6\alpha_{xz}^2 + 6\alpha_{xy}^2 + 6\alpha_{yz}^2 \right]^{\frac{1}{2}}$$

$$\langle\beta\rangle = \left[(\beta_{xxx} + \beta_{xyy} + \beta_{xzz})^2 + (\beta_{yyy} + \beta_{yzz} + \beta_{yxx})^2 + (\beta_{zzz} + \beta_{zxx} + \beta_{zyy})^2 \right]^{\frac{1}{2}}$$

The polarizabilities and hyper polarizability are reported in atomic units (a.u), the calculated values have been converted into electrostatic units (esu) (α : 1 a.u. = 0.1482×10^{-24} esu, β : 1 a.u. = 8.6393×10^{-33} esu). The hyperpolarizability β , dipole moment μ and polarizability α are presented in Table S2. The calculated value of polarizability (α_{zz}) in PAO is 16.3193×10^{-24} esu, predicts highest value compared to other polarizabilities. The magnitude of the molecular hyperpolarizability β , is one of important key factors in a NLO system. The maximum value of dipole moment is calculated in HF/6-311++G(d,p) (0.9609). The highest and lowest hyperpolarizabilities are observed as $232.08891 \times 10^{-33}$ esu and 22.4982×10^{-33} in the direction β_{zyy} and β_{zxx} in HF/6-311++G(d,p).

Natural bond orbital analysis

Natural bond orbital analysis is an essential tool for studying intra- and intermolecular bonding and interaction among bonds, and also provides a convenient basis for investigating charge transfer or conjugative interaction in molecular systems. Some electron donor orbital, acceptor orbital and the interacting stabilization energy resulting from the second-order micro disturbance theory is reported [22,23]. The larger the $E(2)$ value, the more intensive is the interaction between electron donors and electron acceptors, i.e. the more donating tendency from electron donors to electron acceptors and the greater the extent of conjugation of the whole system. Delocalization of electron density between occupied Lewis-type (bond or lone pair) NBO orbitals and formally unoccupied (antibond or Rydberg) non-Lewis NBO orbitals correspond to a stabilizing donor acceptor interaction. The intramolecular interaction are formed by the orbital overlap between $\sigma(\text{C}-\text{C})$, $\sigma^*(\text{C}-\text{C})$, $\pi(\text{C}-\text{C})$, $\pi^*(\text{C}-\text{C})$ bond orbital which results intermolecular charge transfer (ICT) causing stabilization of the system. These interactions are observed as increase in electron density (ED) in C–C anti-bonding orbital that weakens the respective bonds. These intramolecular charge transfer ($\sigma \rightarrow \sigma^*$, $\pi \rightarrow \pi^*$) can induce large

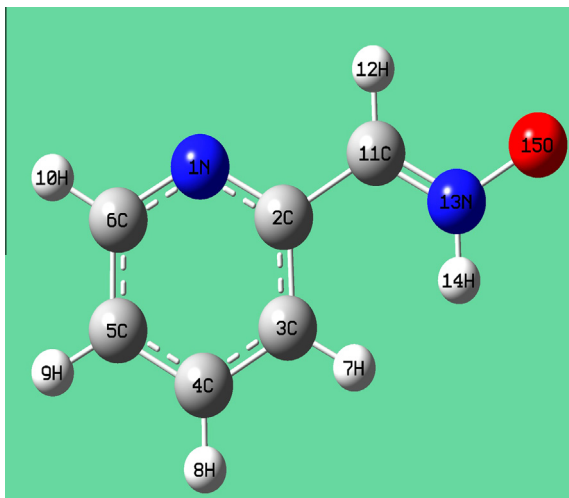


Fig. 3. Optimized geometric structure with atoms numbering of pycolinaldehyde oxime.

nonlinearity of the molecule. The strong intramolecular hyperconjugative interaction of the σ electron of C3–C4 distribute to σ^* C2–C3, C2–C11, C3–H7, C4–C5, C4–H8 and C5–H9 of the ring as evident from Table 1. On the other hand, side the π (C3–C4) in the ring conjugate to the anti-bonding orbital of π^* (N1–C2) and (C5–C6) which leads to strong delocalization of 26.18 and 17.32 kJ/mol. The π (C5–C6) bond is conjugated to the anti-bonding orbital of π^* (N1–C2) and (C3–C4) contributing energy of 18.19 and 22.66 kcal/mol.

Thermodynamic properties

The variation in zero-point vibrational energies (ZPVEs) seems to be significant. The ZPVE is much lower by the DFT B3LYP method than by the HF method. The biggest value of ZPVE of PAO is obtained 1219.178 auk by B3LYP/6-311++G(d,p) whereas the smallest values are 1201.839 a.u. obtained at HF/6-311++G(d,p). Dipole moment reflects the molecular charge distribution and is given as a vector in three dimensions. Therefore, it can be used as descriptor to depict the charge movement across the molecule. The dipole moment vector in a molecule depends on the centers of positive and negative charges. Dipole moments are strictly determined for neutral molecules. For charged systems, its value depends on the choice of origin and molecular orientation. As a result of HF and DFT (B3LYP) calculations the highest dipole moment was observed for HF/6-311G++(d,p) whereas the smallest one was observed for B3LYP/6-311G(d,p) in each molecule. On the basis of vibrational analysis, the statically thermodynamic functions: heat capacity (C), entropy (S), and enthalpy changes (H) for the title molecule were obtained from the theoretical harmonic frequencies and listed in Table 2. It can be observed that these thermodynamic

functions are increasing with temperature ranging from 100 to 500 K due to the fact that the molecular vibrational intensities increase with temperature [24]. The correlation equations between heat capacity, entropy, enthalpy changes and temperatures were fitted by quadratic formulas and the corresponding fitting factors (R^2) for these thermodynamic properties are 0.99234, 0.99994 and 0.99995, respectively. The corresponding fitting equations are as follows and the correlation graphs of those shows in Fig. S1.

$$C = 1.49565 + 0.11612T - 6.8516 \times 10^{-5}T^2 (R^2 = 0.98978)$$

$$S = 52.06744 + 0.11498T - 2.63874 \times 10^{-5}T^2 (R^2 = 0.99994)$$

$$H = 0.22509 + 0.00336T + 4.26517 \times 10^{-5}T^2 (R^2 = 0.99995)$$

All the thermodynamic data supply helpful information for the further study on PAO. They can be used to compute the other thermodynamic energies according to relationships of thermodynamic functions and estimate directions of chemical reactions according to the second law of thermodynamics in Thermo chemical field. Notice: all thermodynamic calculations were done in gas phase and they could not be used in solution.

Mulliken atomic charges

The calculated mulliken charges values natural charges of PAO are listed in Table 3. The results show that substitution of the pyridine ring by oxime group leads to are distribution of electron density. The charges changes with basis set presumably occurs due to polarization, for example, the charge of O15 atom is $-0.2403e^-$ for B3LYP/6-311++G(d,p), $-0.36176e^-$ for HF/6-311++G(d,p) and $-0.5350e^-$ for natural charge. The charge of atom N is positive B3LYP with 6-311++G(d,p) basis set, however in both

Table 1
Second order perturbation theory analysis of Fock matrix in NBO basis for PAO.

Donor (I)	Type of band	Occupancy	Acceptor (J)	Type of band	Occupancy	E2 (kJ/mol) ^a	E (j)–E (i) (a.u) ^b	F (i, j) (a.u) ^c
C2–C11	σ	1.974	N1–C2	σ^*	0.019	0.83	1.16	0.028
		1.974	N1–C6	σ^*	0.508	3.45	1.17	0.057
		1.974	C2–C3	σ^*	0.033	1.00	1.19	0.031
		1.974	C3–C4	σ^*	0.016	2.38	1.20	0.048
		1.974	N13–O15	σ^*	0.014	4.59	0.93	0.058
C2–C3	σ	1.981	N1–C2	σ^*	0.019	2.09	1.24	0.045
		1.981	C2–C11	σ^*	0.035	1.04	1.09	0.030
		1.981	C3–C4	σ^*	0.016	2.89	1.28	0.054
		1.981	C3–H7	σ^*	0.016	1.14	1.16	0.032
		1.981	C4–H8	σ^*	0.013	2.26	1.17	0.046
C3–C4	σ	1.981	C11–H12	σ^*	0.010	0.91	1.15	0.029
		1.979	C2–C3	σ^*	0.033	3.15	1.26	0.056
		1.979	C2–C11	σ^*	0.035	3.11	1.09	0.052
		1.979	C3–H7	σ^*	0.016	1.32	1.16	0.035
		1.979	C4–C5	σ^*	0.015	2.44	1.28	0.050
C3–C4	π	1.979	C4–H8	σ^*	0.013	0.90	1.17	0.029
		1.979	C5–H9	σ^*	0.013	2.34	1.17	0.047
		1.665	N1–C2	π^*	0.439	26.18	0.27	0.077
		1.665	C5–C6	π^*	0.299	17.32	0.28	0.063
		1.980	C3–C4	σ^*	0.016	2.59	1.27	0.051
C4–C5	σ	1.980	C3–H7	σ^*	0.016	2.75	1.15	0.050
		1.980	C4–H8	σ^*	0.013	0.93	1.17	0.029
		1.980	C5–C6	σ^*	0.299	2.11	1.26	0.046
		1.980	C5–H9	σ^*	0.013	1.02	1.17	0.031
		1.980	C6–H10	σ^*	0.022	1.93	1.16	0.042
C5–C6	σ	1.986	N1–C6	σ^*	0.508	1.16	1.24	0.034
		1.986	C4–C5	σ^*	0.015	2.22	1.27	0.047
		1.986	C4–H8	σ^*	0.013	2.50	1.16	0.048
		1.986	C5–H9	σ^*	0.013	0.94	1.17	0.030
		1.986	C6–H10	σ^*	0.022	0.86	1.16	0.028
C5–C6	π	1.622	N1–C2	π^*	0.439	18.19	0.26	0.062
		1.622	C3–C4	π^*	0.302	22.66	0.27	0.072

^a E(2) means energy of hyper conjugative interactions.

^b Energy difference between donor and acceptor i and j NBO orbitals.

^c F(i, j) is the Fock matrix element between i and j NBO orbitals.

Table 2
Thermodynamic functions at different temperatures at the B3LYP/6-311++G(d,p) level for PAO.

T (K)	C (cal mol ⁻¹ K ⁻¹)	S (cal mol ⁻¹ K ⁻¹)	H (cal mol ⁻¹ K ⁻¹)
100	10.942	63.358	0.994
150	18.995	68.559	1.670
200	22.872	74.159	2.620
250	26.002	79.125	3.721
300	29.903	84.186	5.072
350	33.224	89.118	6.639
400	36.520	93.724	8.347
450	39.747	98.577	10.423
500	43.007	102.928	12.547

Table 3
Mulliken atomic charges and Natural charges of PAO.

Atoms	Mulliken charges		Natural charges
	HF/6-311++G(d,p)	B3LYP/6-311++G(d,p)	B3LYP/6-311++G(d,p)
N1	-0.0589	0.0095	-0.4539
C2	-0.3780	-0.4360	0.1482
C3	0.6202	0.6415	-0.2252
C4	-0.8837	-0.9039	-0.1579
C5	0.0367	0.2083	-0.2303
C6	-0.1556	-0.2424	0.0690
H7	0.3463	0.2837	0.1871
H8	0.2245	0.1789	0.2110
H9	0.2181	0.1856	0.2103
H10	0.2243	0.1940	0.1931
C11	-0.2785	-0.2558	0.0703
H12	0.2313	0.1859	0.2262
N13	-0.1140	-0.1010	-0.0790
H14	0.3288	0.2921	0.3660
O15	-0.3618	-0.2404	-0.5350

HF and natural charge with 6-311++G(d,p) this charge is negative. The charge of the nitrogen atom is lowest value in HF/6-311++G(d,p) and highest value in B3LYP/6-311++G(d,p). The charges of atom N13 are $-0.1010e^-$ and $-0.1139e^-$ for B3LYP and HF methods with 6-311++G(d,p), respectively. In C2 carbon atom, the charge distribution is higher value in HF/6-311++G(d,p) basis set and little lower value in B3LYP/6-311++G(d,p). The results show that substitution of the pyridine ring by a oxime group leads to a redistribution of electron density. All the hydrogen atoms have a net positive charge. Moreover, the H8, H9 and H10 atoms in carbon position to (CH=NOH) accommodate higher positive charge than the H7 atom. Considering the all methods and basis sets used in the atomic charge calculation, the oxygen atoms exhibit a negative charge, which are donor atoms. Hydrogen atom exhibits a positive charge, which is an acceptor atom, may suggest the presence of both inter-molecular bonding in the gas phase.

Vibrational analysis

The title molecule consists of 15 atoms, which undergo 39 normal modes of vibrations. The 39 normal modes of PAO are distributed by symmetry species as:

$$\Gamma_{\text{vib}} = 28A' + 11A''$$

It agrees with C_s point group symmetry, all vibrations are active both in Raman and infrared absorption. Here A' represents symmetric planer and A'' asymmetric non planer vibrations. The detailed vibrational assignment of the experimental wavenumbers is based on normal mode analyses and a comparison with theoretically scaled wavenumbers. In Figs. 4 and 5, the calculated frequencies are usually higher than the corresponding experimental quantities, due to the combination of electron correlation effects and basis set

deficiencies. After applying the scaling factors, the theoretical calculations reproduce the experimental data well in agreement. The observed and scaled theoretical frequencies, IR intensities, Raman activities, and mode of description are listed in Table 4.

C–H vibrations

The C–H stretching frequencies appear in the range of 3100–3000 cm^{-1} [25]. The investigated molecule is single substituted, therefore four aromatic C–H vibrations (C3–H7, C4–H8, C5–H9 and C6–H10) plus one (C11–H12) with pyridine substitution were observed in vibrational spectra. From Table 5, the theoretically calculated scaled down vibrations corresponding with C–H stretch show good agreement with the experimentally observed vibrations at 3080(m) and 3040(m) cm^{-1} in FT-Raman and 3090(s), 3050(s) and 3010(s) cm^{-1} in FTIR. The bands are appeared with very strong intensities. It clearly shows that C–H stretching vibrations are not affected by the substitution of an oxime group. The C–H vibrational frequencies are downshifted due to the inductive effect of the aldehyde compound. The calculated frequencies are very good agreement in B3LYP/6-311++G(d,p) basis set for PAO. All the above vibrations are observed in the expected range. Substitution sensitive C–H in-plane bending vibrations lie in the region 1000–1300 cm^{-1} [26]. In PAO, three infrared bands at 1200(s), 1150(vw), 1130(w), 1110(m) and 1050(m) cm^{-1} are assigned to C–H in-plane bending vibrations. All these bands are in the expected range. The upper limit of vibration of the compound is shortened with literature values which may be due to the oxime compounds. Bands involving the out-of-plane C–H vibrations appear in the range 1000–675 cm^{-1} [27]. The C–H out-of-plane bending vibrations are also lie within the characteristic region. However, the change in the frequencies of these deformations from the values in PAO is almost determined exclusively by the relative position of the substituents and is almost independent of their nature. The bands at 880(m), 840(s), 780(m), 760(m) and 710(s) cm^{-1} are assigned to C–H out-of-plane vibrations for PAO.

C–C vibrations

The ring stretching vibrations are very much important in the spectrum of toluene, benzene and their derivatives are highly characteristic of the aromatic ring itself. The bands between 1400 and 1650 cm^{-1} in benzene derivatives are usually assigned to C–C stretching modes [28]. Varsanyi observed five bands, 1625–1590, 1590–1575, 1540–1470, and 1465–1430 and 1380–1280 cm^{-1} , in this region [29]. For title compound, the C–C stretching vibrations are found at 1530(vs), 1490(s) and 1430(s) cm^{-1} in Raman and the C–C stretching vibrations are assigned at 1510(w) and 1500(vs), cm^{-1} in IR. All bands are appeared in the expected range, except first band. Most of the bands are observed with medium and strong intensities. The mean difference between theoretical (B3LYP/6-311++G(d,p)) and experimental frequencies are very less. It shows the good agreement between theoretical and experimental C–C stretching vibrations. The absorption bands arising from C–C in plane bending vibrations are usually observed in the region at 675–1000 cm^{-1} [30]. The two bands (1040, 900) cm^{-1} are in Raman with medium and very strong intensity, and last one is lie in both Raman and IR (1000 cm^{-1}) with medium intensity. This is in agreement with the literature data. The bands are assigned to C–C out-of-plane bending vibrations are observed at 450 and 112 cm^{-1} these vibrations are assigned at 420(s), 390(vs) and 320 (vw) cm^{-1} in IR [31]. The mean difference between experimental and calculated (B3LYP/6-311++G(d,p)) values of C–C vibrations is only 1 cm^{-1} .

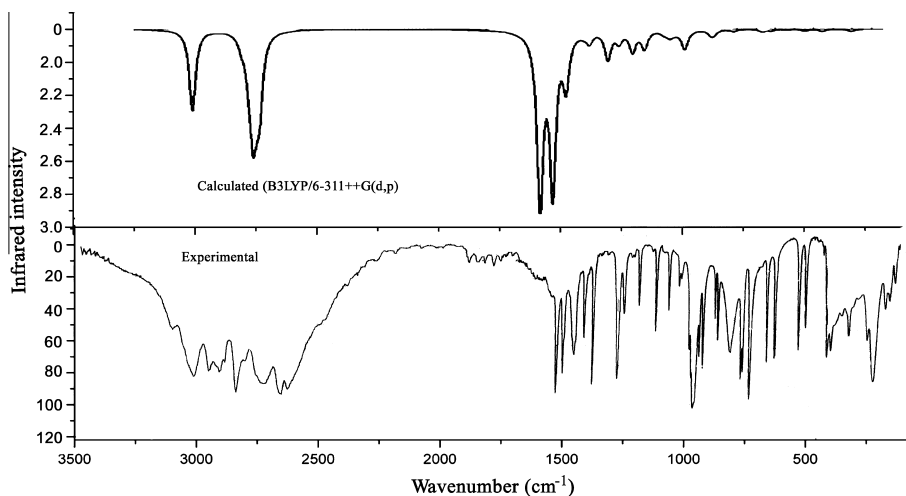


Fig. 4. Experimental and simulated Infrared spectra of pycolinaldehyde oxime.

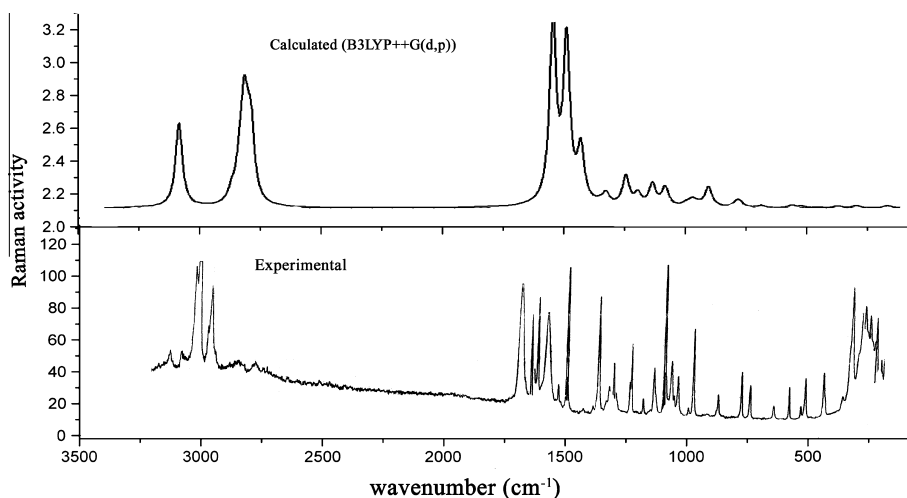


Fig. 5. Experimental and simulated Raman spectra of pycolinaldehyde oxime.

C–N vibrations

Because of the mixing of several bands, the identification of C–N vibrations is a very difficult task. Silverstein assigned C–N stretching absorption in the region $1382\text{--}1266\text{ cm}^{-1}$ [32]. In the present work, the bands are observed at $1380(\text{w})$ and $1320(\text{vs})\text{ cm}^{-1}$ in FT-Raman spectrum has been assigned to C–N stretching vibration. The modes are calculated at 1390 and 1302 cm^{-1} in B3LYP/6-311++G(d,p) basis set which in good agreement with experimental value. The remainder of the observed and calculated wavenumbers and assignments of present molecule are shown in Table 5.

N–O and N–H vibrations

The characteristics group frequencies of the N–O are independent of the rest of the molecule. For the assignments of N–O group frequencies can be associated to symmetric and antisymmetric stretch, in-plane vibrations which scissoring and rocking. In addition to that, wagging and twisting modes would be expected to be depolarized for out-of-plane vibrations. The N–O stretching vibration in aromatic compounds has strong absorption at 960 cm^{-1} [33]. Hence, the asymmetric stretching mode of N–O

group for PAO is identified at $940(\text{w})\text{ cm}^{-1}$ in FTIR spectrum. The symmetric in-plane bending mode of N–H group is assigned at $510(\text{s})\text{ cm}^{-1}$ and out-of-plane $190(\text{m})\text{ cm}^{-1}$ in both FTIR and FT-Raman spectrum respectively. These values are lower than theoretical frequency region [34]. Even N–H stretch, in-plane and out-of-plane vibrations are assigned at $3170(\text{m})$, $1230(\text{s})$ and $950(\text{w})$ in Raman, which is in agreement with the literature data [35]. These bands were also found well within the characteristic region and summarized in Table 5.

Frontier molecular orbitals (FMOs)

The highest occupied molecular orbitals (HOMOs) and the lowest-lying unoccupied molecular orbitals (LUMOs) are named as frontier molecular orbitals (FMOs). The FMOs play an important role in the optical and electric properties, as well as in quantum chemistry and UV–VIS spectra [36]. The HOMO represents the ability to donate an electron, LUMO as an electron acceptor represents the ability to obtain an electron. The energy gap between HOMO and LUMO determines the kinetic stability, chemical reactivity and optical polarizability and chemical hardness–softness of a molecule [37]. In order to evaluate the energetic behavior of the title compound, the HOMO–LUMO energy gap

Table 4
Detailed vibrational assignments of experimental and theoretical wavenumbers of PAO.

Sl. No	S ^y	Experimental ^a		B3LYP/6-311++G(d,p)			Force constants	Vibrational assignment
		FTIR	FTIRaman	Scaled	I ^{IR}	S ^{Raman}		
1	A'		3170(m)	3201	18.61	295.77	7.09	(N–H)ν
2	A'		3090(s)	3096	3.76	33.40	6.73	(C–H)ν
3	A'	3080(m)		3081	7.17	69.12	6.65	(C–H)ν
4	A'		3050(s)	3060	12.87	217.51	6.59	(C–H)ν
5	A'	3040(m)		3042	7.25	81.01	6.47	(C–H)ν
6	A'		3010(s)	3016	21.21	133.60	6.36	(C–H)ν
7	A'		1590(w)	1613	72.08	55.43	5.90	(C=N)ν
8	A'	1530(vs)		1588	46.29	454.36	7.50	(C–C)ν
9	A'		1510(w)	1575	13.56	8.20	7.85	(C–C)ν
10	A'		1500(vs)	1533	35.68	235.94	2.58	(C–C)ν
11	A'	1490(s)		1457	9.06	4.14	2.65	(C–C)ν
12	A'	1430(s)		1438	37.34	37.85	2.70	(C–C)ν
13	A'	1380(w)		1390	216.65	3.68	2.13	(C–N)ν
14	A'	1320(vs)		1302	0.82	62.07	1.94	(C–N)ν
15	A'		1230(s)	1293	0.40	3.97	2.76	(N–H)δ
16	A'	1200(s)		1217	1.03	77.07	2.88	(C–H)δ
17	A'		1150(vw)	1157	2.07	26.81	0.93	(C–H)δ
18	A'		1130(w)	1108	89.42	17.17	1.65	(C–H)δ
19	A'	1110(m)		1093	12.30	2.66	1.18	(C–H)δ
20	A'		1050(m)	1047	8.22	17.74	1.54	(C–H)δ
21	A''	1040(m)		1001	0.73	0.50	0.80	(C–C)δ
22	A'	1000(vw)	1000(m)	987	5.59	53.94	4.34	(C–C)δ
23	A'		950(w)	967	2.23	0.18	0.81	(N–H)γ
24	A''		940(w)	910	9.20	0.17	0.65	(N–O)ν
25	A''	900(vs)	900(s)	886	8.23	0.66	0.62	(C–C)δ
26	A'	880(m)	880(vs)	886	4.55	10.62	2.35	(C–H)γ
27	A''		840(s)	809	88.37	3.61	0.70	(C–H)γ
28	A''	780(s)	780(m)	763	1.03	10.56	2.30	(C–H)γ
29	A'		760(m)	760	2.30	0.01	0.44	(C–H)γ
30	A''		710(s)	741	19.42	0.06	0.85	(C–H)γ
31	A'		620(vs)	624	4.05	4.73	1.72	(C–N)δ
32	A''	560(w)	560(s)	556	1.96	2.05	0.57	(C–N)δ
33	A'	510(w)	510(s)	508	18.11	2.94	1.00	(N–O)δ
34	A''	420(vw)	420(s)	412	4.10	0.60	0.38	(C–C)γ
35	A''		390(m)	389	12.39	1.43	0.30	(C–C)γ
36	A'		320(vw)	337	2.46	6.06	0.52	(C–C)γ
37	A'	190(w)	190(m)	191	12.89	5.31	0.15	(N–O)γ
38	A''	100(vs)	100(s)	162	23.29	0.68	0.06	(C–N)γ
39	A''	80(s)		84	6.47	0.14	0.02	(C–N)γ

S^y: symmetry species; ^as: strong; vs: very strong; m: medium; w: weak; vw: very weak. ν: stretching; δ: in-plane bending; γ: out-of-plane bending; I^{IR}: IR intensity; S^{Raman}: Raman scattering activity.

Table 5
The experimental, calculated and corrected ¹H and ¹³C NMR isotropic chemical shifts (ppm) of PAO.

Atoms	B3LYP		Expt. ^a	Atoms	B3LYP		Expt. ^a
	Calculated	Corrected			Calculated	Corrected	
C2	161.55	154.34	151.61	H14	11.42	12.20	12.06
C11	157.84	150.02	149.58	H10	8.89	8.75	9.02
C6	153.07	144.46	148.71	H12	7.94	8.46	8.13
C4	143.22	132.98	137.26	H8	7.84	7.93	8.02
C3	140.08	129.33	123.88	H9	7.21	7.39	7.30
C5	132.92	120.98	121.17				

was calculated at the B3LYP/6-311++G(d,p) level, which reveals that the energy gap reflects the chemical activity of the molecule. The energies of four important molecular orbitals of PAO in gas: the second highest and highest occupied MO's (HOMO and HOMO–1), the lowest and the second lowest unoccupied MO's (LUMO and LUMO + 1) were calculated. The calculated energy value of HOMO is –8.4510 eV and LUMO is 2.2430 eV in gaseous phase. The value of energy separation between the HOMO and LUMO is 10.6940 eV explains the eventual charge transfer interaction within the molecule, which influences the biological activity of the molecule. Consequently, the lowering of the HOMO ↔ LUMO band gap is essentially a consequence of the

large stabilization of the LUMO due to the strong electron-acceptor ability of the electron-acceptor group. Other quantum descriptors like Electro negativity (χ), Chemical hardness (η), Electrophilicity index (ψ) and Softness (ζ) of PAO is 5.2548, 3.0631, 4.4636, and 0.1616 eV in gas respectively. The 3D plots of the HOMO, HOMO – 1, LUMO and LUMO + 1 orbitals computed at the B3LYP/6-311++G(d,p) level for PAO molecule are illustrated in Fig. 6 (in gas). As can be seen, overlapping of orbital loops located on the HOMO and LUMO confirms the presence a resonance-assisted hydrogen bonding. The positive phase is red (For interpretation of the references to colour in this text, the reader is referred to the web version of the article.) and the

negative one is green. It is clear from the figure that, while the HOMO is localized on the whole molecule which splitted up into two rings, but in LUMO is localized on the pyridine ring and substitution atom, which splitted up into four rings. The HOMO → LUMO transition implies an electron density transfer to CH=NOH atom.

The molecular electrostatic potential (MEP) map is shown in the Fig. 7. It is useful to study the electrophile attracted negative regions (where the electron distribution effect is dominant). In the majority of the MEP, while the maximum negative region which preferred site for electrophilic attack indications as red colour, the maximum positive region which preferred site for nucleophilic attack symptoms as blue colour. The importance of MEP lies in the fact that it simultaneously displays molecular size, shape as well as positive, negative and neutral electrostatic potential regions in terms of colour grading (Fig. 7) and is very useful in research of molecular structure with its physiochemical property relationship. The resulting surface simultaneously displays molecular size and shape and electrostatic potential value.

The different values of the electrostatic potential are represented by different colors. Potential increases in the order red < orange < yellow < green < blue. Regions of negative are usually associated with the lone pair of electronegative atoms. As can be seen from the MEP map of the title molecule, while regions having the negative potential are over the electronegative atoms (C=C group, oxygen and nitrogen atoms), the regions having the positive potential are over hydrogen atoms. The O and N atoms indicates the strongest repulsion with other atoms.

NMR spectra and calculations

The theoretical ^1H and ^{13}C NMR chemical shifts of C and H have been compared with the experimental data [38] as shown in Table 5. Chemical shifts are reported in ppm relative to TMS for ^1H and ^{13}C NMR spectra. The atom statuses were numbered according to Fig. 3. Firstly, full geometry optimization of the PAO was performed at the gradient corrected density functional level of theory using the hybrid B3LYP method based on Becke's three parameters functional of DFT. Then, gauge-including atomic orbital (GIAO) ^1H and ^{13}C chemical shift calculations of the compound was made by the same method using 6-311++G(d,p) basis set IEFPCM/CDCl₃

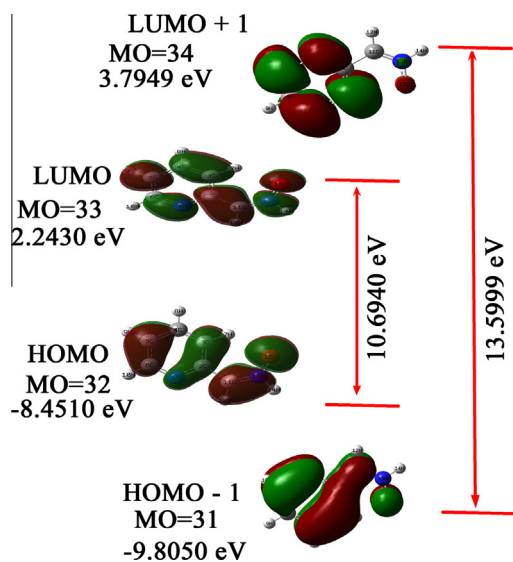


Fig. 6. HOMO and LUMO orbitals of pycolinaldehyde oxime.

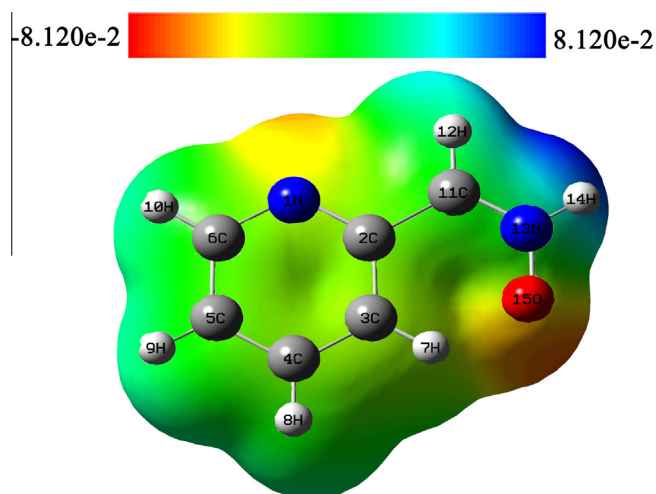


Fig. 7. Molecular electrostatic potential of pycolinaldehyde oxime.

solution. Aromatic carbons give signals in overlapped areas of the spectrum with chemical shift values from 100 to 150 ppm.

In our present investigation, the experimental chemical shift values of aromatic carbons are in the range 121.17–151.61 ppm. The N atom have more electronegative property polarizes the electron distribution in its bond to adjacent carbon atom and decreases the chemical shifts value. The ^1H and ^{13}C NMR isotropic chemical shifts (ppm) of PAO are shown in Fig. 8. On the basis of ^{13}C NMR spectra, in which the ring carbons (C2 and C11) attached to the N atom have bigger chemical shift (161.55 and 157.84 ppm) than the other carbon atoms because of the substitution of NHO group. The chemical shift values of C3 and C5 (140.08 and 132.92 ppm) are smaller than the other aromatic carbons. The experimental chemical shift values of 149.58 ppm (B3LYP) for carbon atom (C11) are in good agreement with the computed values (150.02 ppm).

The chemical shifts obtained and calculated for the ^1H atoms of oxime groups are quite low. Because, the hydrogen atoms are attached to nearby electron-withdrawing atom and group can decrease the shielding. Attached to ring protons are accumulated in the range of 7.21–11.42 ppm (B3LYP), observed experimentally in 7.30–12.06 ppm. The correlations between the experimental and calculated chemical shifts obtained by B3LYP method are shown in Fig. 9. There is a good agreement between experimental and theoretical chemical shift results for the title compound. The performances of the B3LYP method with respect to the prediction of the chemical shifts within the molecule were quite close.

Conclusion

A complete vibrational analysis of PAO are by performed HF and DFT-B3LYP methods with 6-311++G(d,p) basis sets. The influences of substitutions of oxime with ring are investigated and the vibrational frequencies of the title compound are discussed. The observed and stimulated spectra are agreed for the good frequency fit in DFT B3LYP/6-311++G(d,p) method. The less standard deviation between theoretical and experimental wave numbers is confirmed by the qualitative agreement between the calculated and observed frequencies. The MEP map shows the negative potential sites are on oxygen and nitrogen atoms as well as the positive potential sites are around the hydrogen atoms. Furthermore, the thermodynamic properties of the compound are calculated. The correlations between the statistical thermodynamics and temperature are also obtained. It was seen that the heat capacity, entropy

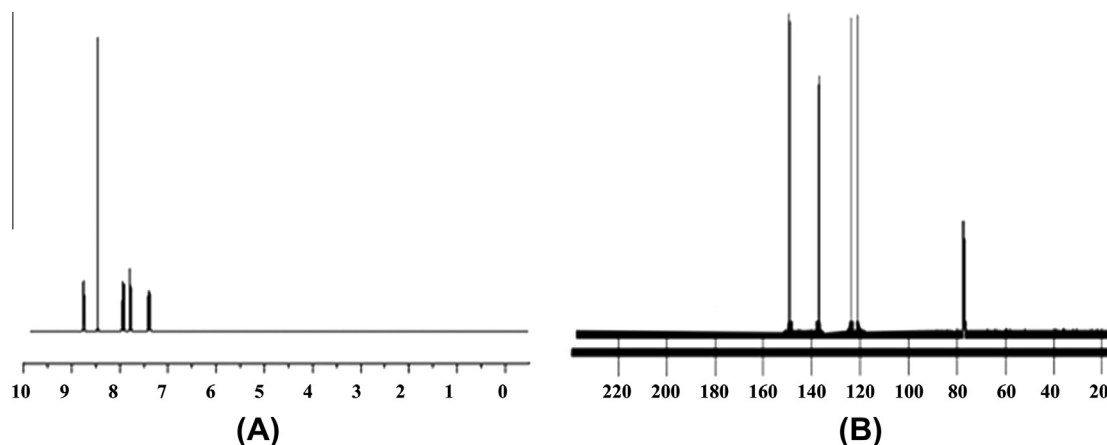


Fig. 8. ^1H and ^{13}C NMR isotropic chemical shifts (ppm) of pycolinaldehyde oxime.

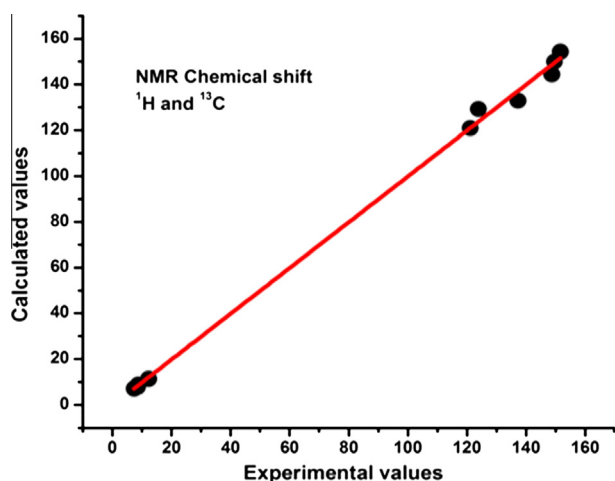


Fig. 9. NMR chemical shift comparison between experimental and calculated frequencies of pycolinaldehyde oxime.

and enthalpy increase with the increasing temperature owing to the intensities of the molecular vibrations increase with increasing temperature. The magnetic properties of title compound are observed and calculated, and chemical shifts are compared with experimental data, showed a good agreement ^1H and ^{13}C NMR. Furthermore, the thermodynamic and electronic absorption properties of the compounds have been calculated. Theoretical electronic absorption spectra have some blue shifts and molecular orbital coefficients analysis suggests that electronic transitions are assigned to $\pi\text{-}\pi^*$ type.

Acknowledgement

The authors gratefully acknowledge the support of this work by the honorable Vice Chancellor and Dean of Periyar Maniyammal University, Vallam, Tanjavur.

Appendix A. Supplementary material

Supplementary data associated with this article can be found, in the online version, at <http://dx.doi.org/10.1016/j.saa.2013.07.080>.

References

- [1] Linnell, Robert, *J. Org. Chem.* 25 (2) (1960) 290.
- [2] A. Kaminski, T. Kino, T. Tama, A. Yukon, K. Ueda, K. Taka chi, J. Hollinger, H.J. Richler, J. Hausa, J. Fernandez, R. Bald, M. Macke, G.M.A. Gad, *Jon. J. Appl. Phys* 41 (2002). L603–L605.
- [3] M. Komati, K. Takahashi, T. Doi, Y. Takimoto, *Anal. Chem.* 69 (1997). 2919–2926.
- [4] C.B. Millard, C.A. Broomfield, *J. Neurochem.*, 1995 (Wiley Online Library).
- [5] M.Y. Li, P.Z. Hu, W.R. Zhu, K.X. Xu, *Chin. Chem. Lett.* 14 (2003) 572–574.
- [6] M. Jokanović, M. Prostran, *Curr. Med. Chem.* 16 (17) (2009) 217788.
- [7] S.P. Jose, S. Mohan, *Spectrochim. Acta* 64A (2006) 240–245.
- [8] K. Othmer, *Encyclopedia of Chemical Technology*, 4th ed., vol. 10, 1997.
- [9] P. Pierrat, P.C. Gros, Y. Fort, *J. Comb. Chem.* 7 (2005) 879–886.
- [10] K.B. Wiberg, V.A. Walters, K.N. Wong, S.D. Colson, *J. Phys. Chem.* 88 (1984) 6067–6075.
- [11] T. Yamamoto, R. Mitsuhashi, M. Akiyama, Y. Kakiuti, *J. Mol. Spectrosc.* 117 (1986) 30–37.
- [12] A. Destexhe, J. Smets, L. Adamowicz, G. Maes, *J. Phys. Chem.* 98 (1994) 1506–1514.
- [13] N. Sundaraganesan, S. Ilakiamani, H. Saleem, M. Piotr, *Spectrochim. Acta Part A* 61 (2005) 2995–3001.
- [14] Z. Zhuang, J. Cheng, X. Wang, B. Zhao, X. Han, Y. Luo, *Spectrochim. Acta Part A* 67 (2007) 509–516.
- [15] D. Nachmansonn, S.Ginsburg, U.S. Patent 2,816,113, 1957.
- [16] E.H. Brennie Jr, Daniher, A. Francis, Ash* Arthur B1 (1966).
- [17] Gaussian 03, Gaussian, Inc., Pittsburgh, PA, 2003.
- [18] M. Karabacak, M. Kurt, *Spectrochim. Acta A* 71 (2008) 876–883.
- [19] M.H. Jamroz, *Vibrational Energy Distribution Analysis VEDA 4*, Warsaw, 2004.
- [20] R.I. Dennington, T. Keith, J. Millam, K. Eppinnett, W. Hovell, Gauss View Version, 2003.
- [21] C. Arunagiri, M. Arivazhagan, A. Subashini, *Spectrochim. Acta A* 79 (2011) 1747–1756.
- [22] C. James, A. AmalRaj, R. Reghunathan, I. Hubert Joe, V.S. JayaKumar, *J. Raman Spectrosc.* 37 (2006) 1381–1392.
- [23] L.J. Na, C.Z. Rang, Y.S. Fang, *J. Zhejiang Univ. Sci.* 6B (2005) 584–589.
- [24] J. Bevan Ott, J. Boerio-Goates, *Calculations from Statistical Thermodynamics*, Academic Press, 2000.
- [25] V. Krishnakumar, R.J. Xavier, *Indian J. Pure Appl. Phys.* 41 (2003) 597.
- [26] G. Socrates, *Infrared and Raman Characteristic Group Frequencies – Tables and Charts*, 3rd ed., Wiley, New York, 2001.
- [27] T.F. Ardyukoiva et al., *Atlas of Spectra of Aromatic and Heterocyclic Compounds*, Nauka Sib otd, Novosibirsk, 1973.
- [28] G. Varsanyi, *Assignments of Vibrational Spectra of 700 Benzene Derivatives*, Wiley, New York, 1974.
- [29] M. Chao, E. Schempp, *Acta Crystallogr.* B33 (1977) 1557.
- [30] S. Gunesekaran, R. Thilak Kumar, S. Ponnusamy, *Spectrochim. Acta Part A* 65 (2006) 1041.
- [31] R.M. Silverstein, G.C. Bassler, T.C. Morrill, *Spectrometric identification of organic compounds*, 3rd ed., John Wiley & Sons, New York, NY, 1974. 239.
- [32] N. Prabavathi, V. Krishnakumar, *Spectrochim. Acta Part A* 72 (2009) 743.
- [33] S. Dheivamalar, V. Krishnakumar, *Spectrochim. Acta Part A* 71 (2008) 465.
- [34] S. Manohar, R. Nagalakshmi, V. Krishnakumar, *Spectrochim. Acta Part A* 71 (2008) 110.
- [35] M. Govindarajan, K. Ganasan, S. Periandy, M. Karabacak, S. Mohan, *Spectrochim. Acta A* 77 (2010) 1005–1013.
- [36] I. Fleming, *Frontier Orbitals, Organic Chemical Reactions*, Wiley, London, 1976.
- [37] B. Kosar, C. Albayrak, *Spectrochim. Acta Part A* 78 (2011) 160–167.
- [38] Spectral Database for Organic Compounds, SDDBS. http://riodb01.ibase.aist.go.jp/sdbs/cgi-bin/direct_frame_top.cgi.